





OPEN

## Structural modeling of GSK3 $\beta$ implicates the inactive (DFG-out) conformation as the target bound by TDZD analogs

Meenakshisundaram Balasubramaniam<sup>1,2</sup>, Nirjal Mainali<sup>3</sup>, Suresh Kuarm Bowroju<sup>5</sup>, Paavan Atluri<sup>4</sup>, Narsimha Reddy Penthal<sup>5</sup>, Srinivas Ayyadevera<sup>1,2</sup>, Peter A. Crooks<sup>5</sup> & Robert J. Shmookler Reis<sup>1,2</sup>

Glycogen synthase kinase-3 $\beta$  (GSK3 $\beta$ ) controls many physiological pathways, and is implicated in many diseases including Alzheimer's and several cancers. GSK3 $\beta$ -mediated phosphorylation of target residues in microtubule-associated protein tau (MAPTAU) contributes to MAPTAU hyperphosphorylation and subsequent formation of neurofibrillary tangles. Inhibitors of GSK3 $\beta$  protect against Alzheimer's disease and are therapeutic for several cancers. A thiadiazolidinone drug, TDZD-8, is a non-ATP-competitive inhibitor targeting GSK3 $\beta$  with demonstrated efficacy against multiple diseases. However, no experimental data or models define the binding mode of TDZD-8 with GSK3 $\beta$ , which chiefly reflects our lack of an established inactive conformation for this protein. Here, we used metadynamic simulation to predict the three-dimensional structure of the inactive conformation of GSK3 $\beta$ . Our model predicts that phosphorylation of GSK3 $\beta$  Serine9 would hasten the DFG-flip to an inactive state. Molecular docking and simulation predict the TDZD-8 binding conformation of GSK3 $\beta$  to be inactive, and are consistent with biochemical evidence for the TDZD-8-interacting residues of GSK3 $\beta$ . We also identified the pharmacophore and assessed binding efficacy of second-generation TDZD analogs (TDZD-10 and Tideglusib) that bind GSK3 $\beta$  as non-ATP-competitive inhibitors. Based on these results, the predicted inactive conformation of GSK3 $\beta$  can facilitate the identification of novel GSK3 $\beta$  inhibitors of high potency and specificity.

Glycogen synthase kinase-3 beta (GSK3 $\beta$ ) is a serine/threonine protein kinase expressed ubiquitously in mammalian cells. GSK3 $\beta$  regulates many physiological pathways by phosphorylating key downstream targets. The kinase activity of GSK3 $\beta$  is implicated in many cancers and in neurodegenerative diseases, including Alzheimer's and Parkinson's diseases<sup>1-3</sup>. For instance, GSK3 $\beta$ -mediated hyperphosphorylation of two key residues, Ser202 and Thr205, of the microtubule-associated protein tau (MAPT or TAU)<sup>4</sup> alters microtubule structure and function. This contributes critically to the formation of hyperphosphorylated tau (hP-tau) and initiates the accrual of paired helical filaments that comprise the neurofibrillary tangles (NFTs), which are specifically recognized by antibody AT8<sup>5</sup>. The presence and high abundance of such tangle-bearing neurons is a neuropathological hallmark of Alzheimer's disease<sup>6</sup>. Hyperphosphorylation of tau, triggered by either MAPK-p38 as previously reported<sup>7</sup> or by GSK3 $\beta$  as shown here, is associated with decreased interactions of tau with microtubules and results in destabilization of microtubules and subsequent decrease in the efficient transport of organelles, proteins, etc., within the neuron<sup>8</sup>.

GSK3 $\beta$  resembles other serine/threonine protein kinases in structure, showing a conserved catalytic domain comprising an N-terminal glycine-rich loop region that is connected by a "hinge" to a C-terminal lobe<sup>9,10</sup>. A highly conserved loop within the C-terminal domain, termed the "activation loop," contains an invariant "DFG"

<sup>1</sup>McClellan Veterans Medical Ctr., Central Arkansas Veterans Healthcare Service, Little Rock, AR 72205, USA. <sup>2</sup>Department of Geriatrics, Reynolds Institute on Aging, University of Arkansas for Medical Sciences, Little Rock, AR 72205, USA. <sup>3</sup>Bioinformatics Program, University of Arkansas for Medical Sciences, and University of Arkansas At Little Rock, Little Rock, AR 72205, USA. <sup>4</sup>Summer Research Internship Program, University of Arkansas for Medical Sciences, Little Rock, AR 72205, USA. <sup>5</sup>Department of Pharmaceutical Sciences, College of Pharmacy, University of Arkansas for Medical Sciences, Little Rock, AR 72205, USA. ✉email: mbalasubramaniam@uams.edu; rjsr@uams.edu

motif (Asp-Phe-Gly), which plays a key role in determining kinase activity. Based on the structural orientation of this conserved Phe and Asp, protein kinases can be distinguished in two conformations, i.e., “active” (“DFG-*in*”) or “inactive” (“DFG-*out*”)<sup>9,11</sup>. When the kinase is in its active conformation, mostly determined by phosphorylation of a tyrosine residue in the activation loop, ATP (adenosine triphosphate) binds to the conserved active-site pocket between the *N*-terminal glycine-rich loop and the C-terminal lobe<sup>12</sup>. The first crystal structure of an inactive kinase conformation was determined for tyrosine-protein kinase Src (*c*-Src), a proto-oncogene. This structure showed Asp and Phe residues rotated ~ 180° relative to their orientations in the active conformation, a flip shared by several other kinases in their crystallography-based inactive conformations<sup>9</sup>. Active and inactive conformations of all kinases are determined primarily by the orientations of Asp (D) and Phe (F) sidechains in the DFG motif<sup>12</sup>. In the active state, Phe in the activation-loop DFG extends its sidechain inward (toward the  $\alpha$ C-helix at the *N*-terminus), while the Asp sidechain faces outward (away from the  $\alpha$ C-helix); this motif orientation is denoted as “DFG-*in*”<sup>13</sup>. In the inactive conformation, Phe flips to face outward while Asp rotates to face inward, denoted as “DFG-*out*”<sup>11,13</sup>. This DFG flip creates an allosteric hydrophobic pocket in the inactive state, adjacent to the ATP-binding region<sup>9,11</sup>.

Several potent kinase inhibitors, including imatinib, have been reported to bind to kinases that are in their inactive conformation. Energetically, kinase inhibition can be most efficiently achieved by stabilizing the allosteric pocket of the inactive conformation (ATP-noncompetitive inhibitors), whereas inhibitors that block the ATP-binding pocket (ATP-competitive inhibitors) must compete with an abundant supply of endogenous ATP<sup>9,11,14</sup>. Therefore, accurate modeling of a target kinase’s inactive conformation is crucial for the design of target-specific inhibitors. Since kinases oscillate between active and inactive conformations, elucidating experimental models is challenging.

GSK3 $\beta$  is thought to be constitutively active in its native form, and is inactivated upon cell stimulation by insulin<sup>15</sup>. Scarcity of the inactive form, and the inherent structural instability of its activation loop, pose major obstacles to molecular modeling based on X-ray crystallography. Notwithstanding its allegedly constitutive activity, the presence of DFG residues in the GSK3 $\beta$  activation loop suggests a potential for inactivation via a DFG-flip. Phosphorylation of Ser9 was shown to inactivate GSK3 $\beta$ <sup>16</sup>, and to inhibit substrate binding<sup>17,18</sup>, leading us to speculate that this phosphorylation may induce a DFG flip.

Selective ATP-noncompetitive inhibitors, including TDZD-8, were proposed to act at the allosteric hydrophobic pocket of GSK3 $\beta$ <sup>19,20</sup>, which is only present in the inactive state. However, the mechanism by which known GSK3 $\beta$  ATP-noncompetitive inhibitors bind to the allosteric pocket of GSK3 $\beta$  remains to be elucidated. Mechanistic studies have been hindered by the lack of a structural model for GSK3 $\beta$  in its inactive conformation, impeding drug development by the usual methods, i.e., lead optimization based on the binding mode of a parent compound such as TDZD-8. For example, the TDZD analog Tideglusib is a potent ATP-noncompetitive GSK3 $\beta$  inhibitor. Tideglusib is known to inhibit GSK3 $\beta$  irreversibly, suggesting the possibility of covalent interaction between the drug (Tideglusib) and the protein (GSK3 $\beta$ )<sup>20</sup>. However, in the absence of an experimental structure for GSK3 $\beta$  binding to Tideglusib, it has not been possible to visualize or identify the site of covalent bond formation. Since Tideglusib is a TDZD analog and is proposed to act as ATP-noncompetitive inhibitor<sup>20</sup>, it is expected to bind to the allosteric pocket of GSK3 $\beta$ . Without structural details, exemplifying binding modes of potent compounds is tedious. Defining the binding mode of inhibitors such as Tideglusib is crucial to understanding its mechanism of action, its pharmacophore, and the key residues of GSK3 $\beta$  involved. This pivotal information is required to develop potent second-generation drugs, capable of inhibiting GSK3 $\beta$  specifically with minimal off-target effects. We now propose a structure for GSK3 $\beta$  in the inactive DFG-*out* conformation, which has been derived from metadynamic-simulation modeling. Several validation procedures support this predicted inactive conformation of GSK3 $\beta$ , which can be retrieved from this site: <https://data.mendeley.com/datasets/d69pzg3syh/1>.

## Results

**Metadynamic-simulation modeling predicts the inactive conformation of GSK3 $\beta$ .** To model the inactive conformation of GSK3 $\beta$ , we began by considering its active conformation. Since the experimentally derived crystal structure of GSK3 $\beta$  omits several loops, we filled these gaps by template modeling (using the template PDB-ID: *Iiep*) followed by loop refinement (Fig. 1a). The resulting structure of the activation loop predicts an outward orientation of aspartic acid D200, away from the ATP binding site, coupled to inward orientation of phenylalanine F201, facing the ATP pocket and the *N*-terminal  $\alpha$ C-helix, i.e., the classical DFG-*in* conformation of active kinases (Fig. 1b). In order to evaluate the model that we generated and the computational parameters employed, we performed virtual docking of ATP with the modeled active conformation of GSK3 $\beta$ . Results obtained for binding of ATP to this predicted active conformation agree well with the experimentally determined active conformation of GSK3 $\beta$  (PDB-ID *Ii09*) depicted in Fig. 1c.

We next attempted to model the inactive conformation of GSK3 $\beta$  by enhanced-sampling metadynamic simulation of the active conformation (see “Methods” for detailed procedures). In brief, the active conformation of GSK3 $\beta$  (Fig. 1a) was immersed in an orthorhombic box containing water plus salt ions (Na<sup>+</sup>, Cl<sup>-</sup>). The distance between the centers of mass of Phe200 and Ser168 was defined as a collective variable (CV) for metadynamic calculations. Simulation, conducted for 100 ns after equilibration, indicated a transition after ~ 18 ns involving both Phe and Asp in the DFG loop (Fig. 1d–e). At 10–25 ns, the DFG active conformation converted to the inactive conformation, i.e., Phe201 flipped almost 180° to face outwards (Fig. 1f), while Asp200 rotated inward 180° (Fig. 1g). Structural-alignment comparisons of this predicted DFG-inactive conformation demonstrated close agreement with the experimentally determined inactive conformations of other kinases, including ABL and AKT (Supplementary Fig. 1). Interestingly, our metadynamic simulation predicting the DFG-flip in GSK3 $\beta$  adopted an intermediate “*up*” conformation of Phe201 during transition to the *out* state (Fig. 1h–j; Supplementary

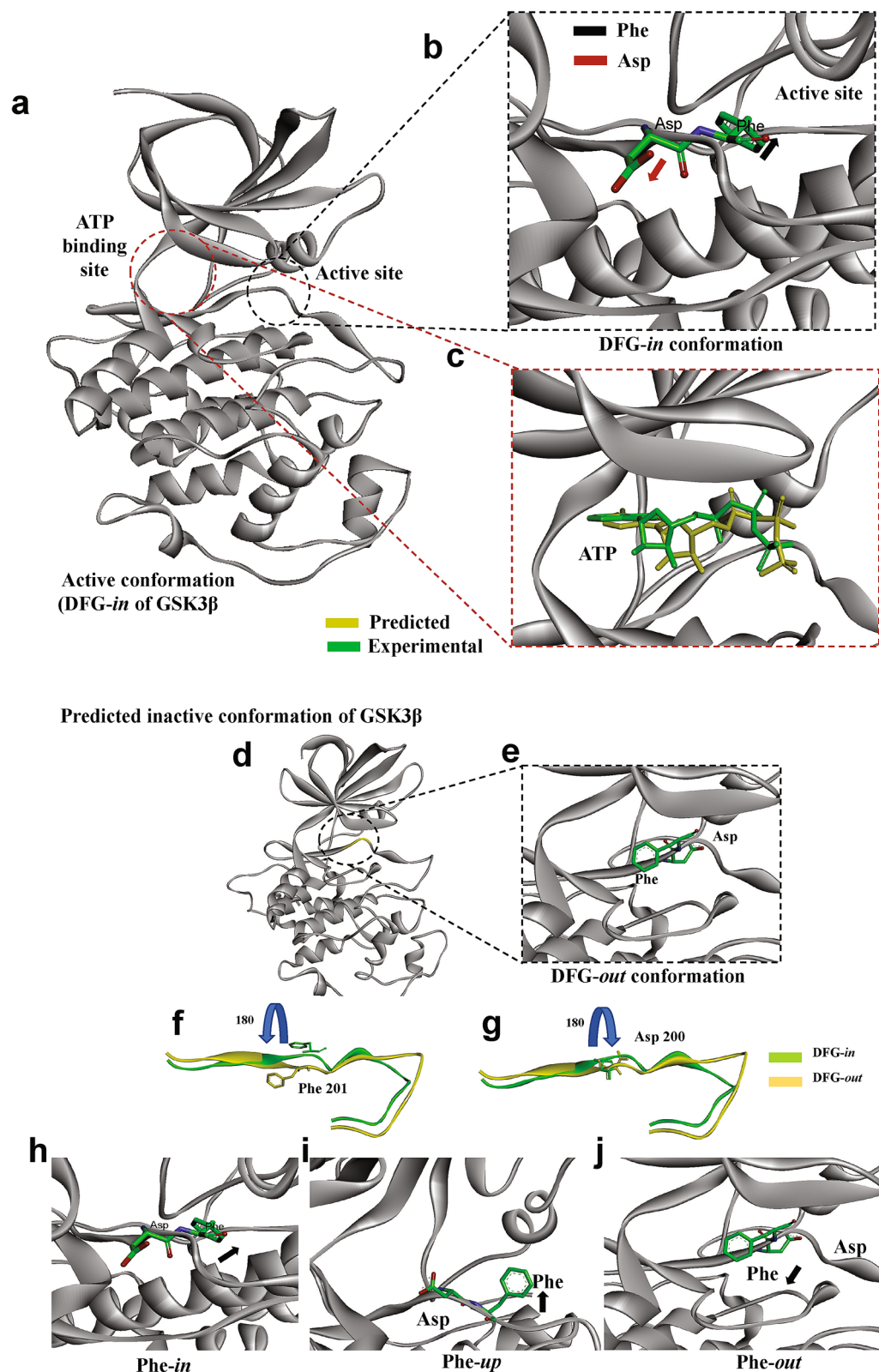


**Figure 1.** Active and inactive conformations of GSK3 $\beta$ . (a) Structure of active GSK3 $\beta$ , based on X-ray crystallography, showing the activation loop in the DFG-*in* conformation. (b) Stick representation of GSK3 $\beta$  residues Asp and Phe, showing the classical active (DFG-*in*) conformation, in which the Asp sidechain is rotated *out* and the Phe ring is turned *in* with respect to the active site. (c) Protein-ligand docking depicts ATP binding within its GSK3 $\beta$  binding site as predicted (yellow ATP structure) in close agreement with experimental data (green ATP). (d, e) Ribbon model of GSK3 $\beta$  inactive (DFG-*out*) conformation, in which Phe201 and Asp200 have rotated (flipped) their orientations relative to the active state. (f, g) Detail from (e), contrasting ribbon models of Phe201 and Asp200 in their active (green) vs. inactive (yellow) orientations, based on metadynamic simulation. (h–j) During metadynamic simulation, the transition of Phe201 from *in* to *out* conformation passes through an intermediate *up* orientation. Molecular structure depictions were created using the BIOVIA Discovery Studio Visualizer 2017 (Dassault Systemes; <https://discover.3ds.com/discovery-studio-visualizer-download>).

Video S1). This transient *up* conformation was previously reported for several kinases, including the Aurora-A and Aurora-B kinases<sup>11,21</sup>.

In order to assess the reliability of the metadynamics approach as a means to predict the DFG-*out* conformation from the DFG-*in* structure, we used c-Abl kinase as a positive control. Since both the DFG-*in* (active) and DFG-*out* (inactive) conformations of c-Abl kinase have been resolved experimentally through X-ray crystallography, we began with the c-Abl kinase DFG-*in* crystal structure (PDBid: 3KF4) and repeated the identical steps used for GSK3 $\beta$ , to ask whether the predicted DFG-*out* conformation agreed with that empirically established crystal structure. As previously, the distance between the Phe381 and Ala350 centers of mass was defined as a collective variable (CV) for metadynamic calculations. Metadynamic simulation commencing with the c-Abl kinase DFG-*in* conformation predicts that a DFG-flip will occur at ~10–20 ns (Supplementary Fig. 2a–c), giving rise to a predicted DFG-*out* conformation that agrees remarkably well with the experimentally determined DFG-*out* structure of c-Abl (PDBid: 3KFA; Supplementary Fig. 2d).

**GSK3 $\beta$  transition to the inactive conformation creates a new hydrophobic/allosteric pocket.** Most kinases, in the inactive conformation, form a hydrophobic binding site adjacent to the ATP-binding pocket, termed the allosteric site<sup>11–13</sup>. Rotation of Asp and Phe in the DFG motif opens up a hydrophobic space between the *N*-terminal and C-terminal lobes<sup>9</sup>. Type-II kinase inhibitors, such as imatinib, generally target the inactive conformation of kinases, by interacting with the hydrophobic binding site (allosteric site) formed after DFG flip<sup>9,13</sup>. In order to ascertain whether our predicted inactive conformation incorporated this hydrophobic binding site, we modeled possible binding cavities in both the active and predicted inactive conformations. Results show a large cavity at the ATP-binding pocket in the active conformation of GSK3 $\beta$  (Fig. 2a, red dashed circle), which is absent in the predicted inactive conformation (Fig. 2b; red dashed circle). At the same time, the transition from active to inactive structures created a new hydrophobic area immediately adjacent to the ATP-binding pocket (Fig. 2b; black dashed circle), not seen in the active conformation (Fig. 2a; black dashed circle). These results lend indirect support for the DFG-flip predicted by metadynamic simulation, and are consistent with this being the true inactive conformation of GSK3 $\beta$ .

**Unphosphorylated Serine 9 delays the DFG flip (inactivation) in GSK3 $\beta$  simulations.** Ser9 plays a critical role in GSK3 $\beta$  activity; its phosphorylation reduces the kinase activity of GSK3 $\beta$ , thereby suppressing phosphorylation of its downstream targets. However, the role of Ser9 phosphorylation in the DFG flip remains to be elucidated, in large part because most available experimental models of GSK3 $\beta$  omit the first 35 *N*-terminal residues. Therefore, using *ab initio* and fold-recognition protocols, we modeled the complete GSK3 $\beta$  structure (hereafter referred to as “full-length GSK3 $\beta$ ”) including the *N*-terminal 35 residues (Fig. 2c). Structural analysis indicates that this modeled GSK3 $\beta$  assumes the active DFG-*in* conformation, and the position of the critical Ser9 in our full-length structural model agrees with the structure reported by Stamos et al.<sup>22</sup>.

We conducted a molecular-dynamic simulation of full-length GSK3 $\beta$  structural variation in the active conformation, using metadynamic simulation with the parameters noted above, including the same collective variable (CV) used previously to maintain consistency. In parallel, we phosphorylated full-length GSK3 $\beta$  at Ser9 (denoted as pSer9) using the Vienna PTM server (<https://vienna-ptm.univie.ac.at/>), and performed molecular simulation by the Metadynamics technique (see “Methods”)<sup>11</sup>. Both unphosphorylated and phosphorylated GSK3 $\beta$  models underwent a structural transition in the DFG region (Fig. 2d–e), from active to inactive conformation. However, this transition was delayed for full-length GSK3 $\beta$  with unphosphorylated Ser9, by ~40 ns relative to either phosphorylated full-length GSK3 $\beta$  (pSer9; Supplementary Fig. 3a–b) or GSK3 $\beta$  lacking the *N*-terminal 35 residues (18–25 ns). Trajectory analysis revealed high instability (structural fluctuation) of the activation loop in unphosphorylated GSK3 $\beta$ , which was stabilized in pSer9-GSK3 $\beta$  (Supplementary Fig. 3a–b). The allosteric pocket formed during DFG transition includes a much smaller volume when GSK3 $\beta$  is unphosphorylated, relative to full-length GSK3 $\beta$  containing pSer9 (Supplementary Fig. 3c–e).

**TDZD-8 protects against aggregation in neurodegenerative models.** Previous studies have shown that TDZD-8 inhibits GSK3 $\beta$  and thus protects against tau hyperphosphorylation<sup>23</sup>, and that other small-molecule inhibitors of GSK3 $\beta$  protect against A $\beta$ <sub>42</sub> aggregation to form  $\beta$ -amyloid<sup>24,25</sup>. We assessed the ability of TDZD-8 to protect human cells against tau aggregation in HEK-tau embryonic kidney cells expressing a MAP-TAU transgene. Thioflavin-T-positive AD-like aggregates were significantly reduced in HEK-tau cells by 5- $\mu$ M TDZD-8 (Fig. 3a,b), consistent with GSK3 $\beta$  playing a critical role in AD-like aggregation.

In addition to this cell model of AD neuropathy, we also assessed a nematode model of Huntington’s disease (*Caenorhabditis elegans* strain AM141), expressing an array of 40 glutamines fused to Yellow Fluorescent Protein (Q40::YFP). Interestingly, even without dose optimization, TDZD-8 treatment substantially attenuated aggregate accumulation in this model, suggesting the possibility that GSK3 $\beta$  or its downstream targets may also be involved in Huntington’s and/or other polyglutamine-array-expansion diseases (Fig. 3c,d).

**TDZD-8 binds to the inactive conformation of GSK3 $\beta$ .** Having now modelled full-length GSK3 $\beta$  in both the active and inactive conformations, we simulated its interaction with TDZD-8 in order to clarify the mode of drug binding. We began with the full-length active conformation of GSK3 $\beta$ , and used Glide to perform protein–ligand targeted docking within the previously proposed TDZD-8-binding region of GSK3 $\beta$ <sup>19</sup>. TDZD-8 was not a good fit to the proposed region (the area around the allosteric/hydrophobic pocket) of the GSK3 $\beta$  active conformation (Supplementary Fig. 4), presumably because this (active) conformation does not form a stable hydrophobic pocket (Fig. 2a). To determine whether TDZD-8 binds to any region of the GSK3 $\beta$  active conformation beyond the proposed pocket, we employed AutoDock-Vina to perform unbiased dock-

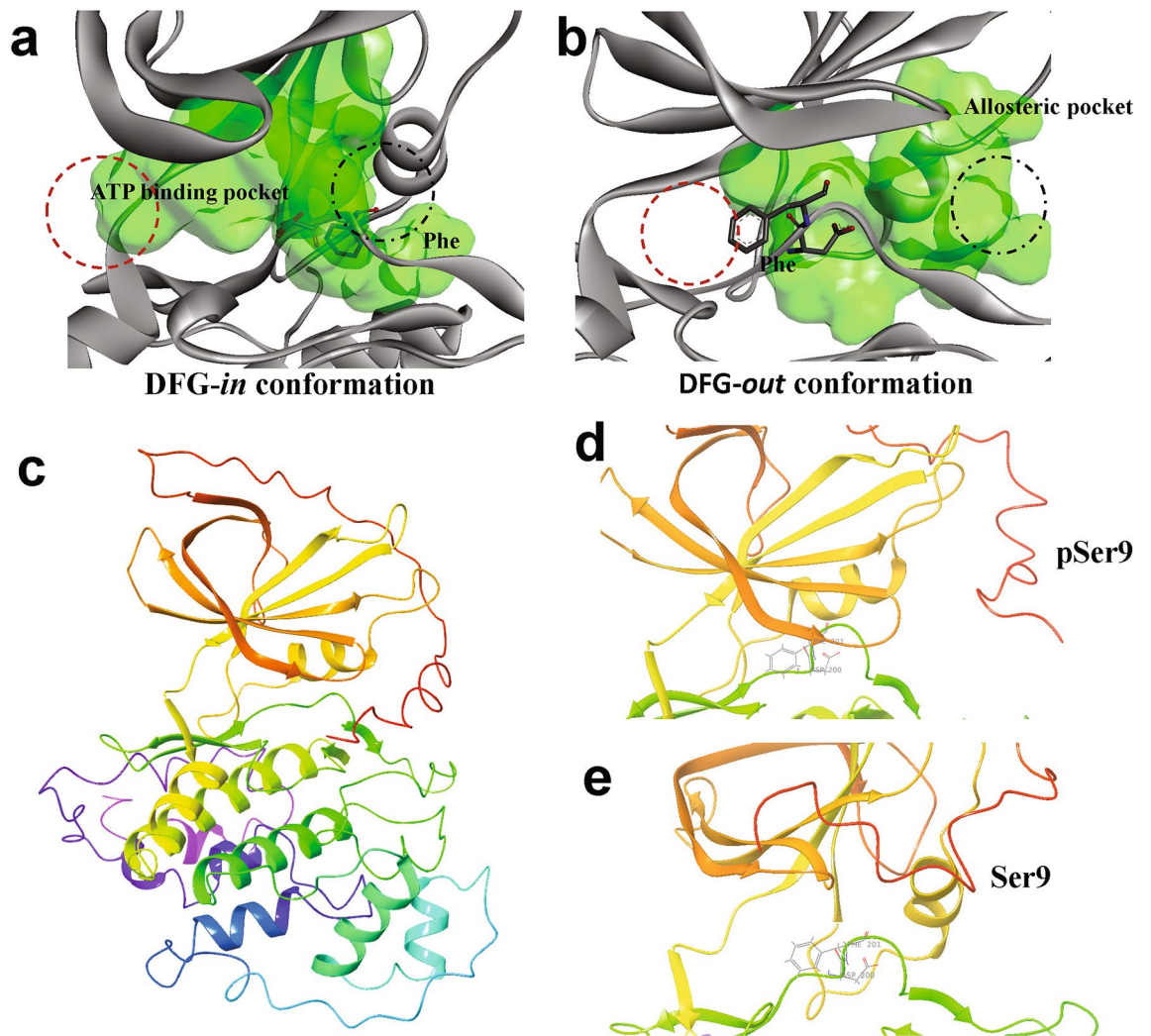


**Figure 2.** Modelled inactive (DFG-out) conformation of GSK3 $\beta$  shows structural changes near the active site. (a) Molecular surface representation (green) of predicted ATP-binding pocket when GSK3 $\beta$  is in the active conformation (DFG-in). (b) GSK3 $\beta$  spontaneously flips the DFG motif to the out (inactive) conformation during metadynamic simulation. The ATP-binding pocket is marked by a red dashed circle, whereas the allosteric hydrophobic pocket is designated by a black dashed circle. (c–e) Structural representations of modelled GSK3 $\beta$  (residues 1–384) in the inactive DFG-out conformation, with Serine9 either phosphorylated (d) or unphosphorylated (e). Molecular structure representations were created using the BIOVIA Discovery Studio Visualizer 2017 (Dassault Systemes; <https://discover.3ds.com/discovery-studio-visualizer-download>), and Schrödinger Maestro 11.4 (<https://www.schrodinger.com/>).

ing, wherein the entire active conformation of full-length GSK3 $\beta$  is enclosed in the docking box<sup>26</sup>. None of the predicted docking poses resulted in TDZD-8 binding to the proposed allosteric/hydrophobic site of GSK3 $\beta$  in the active conformation (data not shown). Although unbiased docking indicates modest TDZD-8 affinity for the ATP-binding pocket of the active-conformation GSK3 $\beta$  (Supplementary Fig. 4), calculation of the solvent-based binding free energy (by the MMGBSA approach<sup>27,28</sup>) predicted that the binding affinity of TDZD-8 for this pocket would be less than half that of ATP (Supplementary Fig. 4d). This indicates that the drug could not compete effectively for the ATP binding site, consistent with previous biochemical evidence that TDZD-8 is an ATP-noncompetitive inhibitor<sup>29</sup>.

Since the proposed hydrophobic pocket in GSK3 $\beta$  is only present when the kinase is in the inactive conformation, we subjected that model to unbiased docking followed by target-specific docking of TDZD-8, as described above. In both procedures, TDZD-8 showed stable binding to the hydrophobic pocket adjacent to the ATP-binding site (Fig. 4a–d). Notably, TDZD-8 binding to this pocket is identical for the predicted inactive conformations of both full-length GSK3 $\beta$  and its truncated form, which lacks the N-terminal 35 residues (Fig. 4a–d). Analysis of the contact residues agrees with the binding mode proposed previously for TDZD-8 interaction with GSK3 $\beta$ <sup>19</sup>. We calculated the solvent-based binding free energy ( $\Delta G_{\text{binding}}$ ) of TDZD-8 targeted to the hydrophobic/allosteric pocket residues, using MMGBSA (molecular mechanics under the generalized

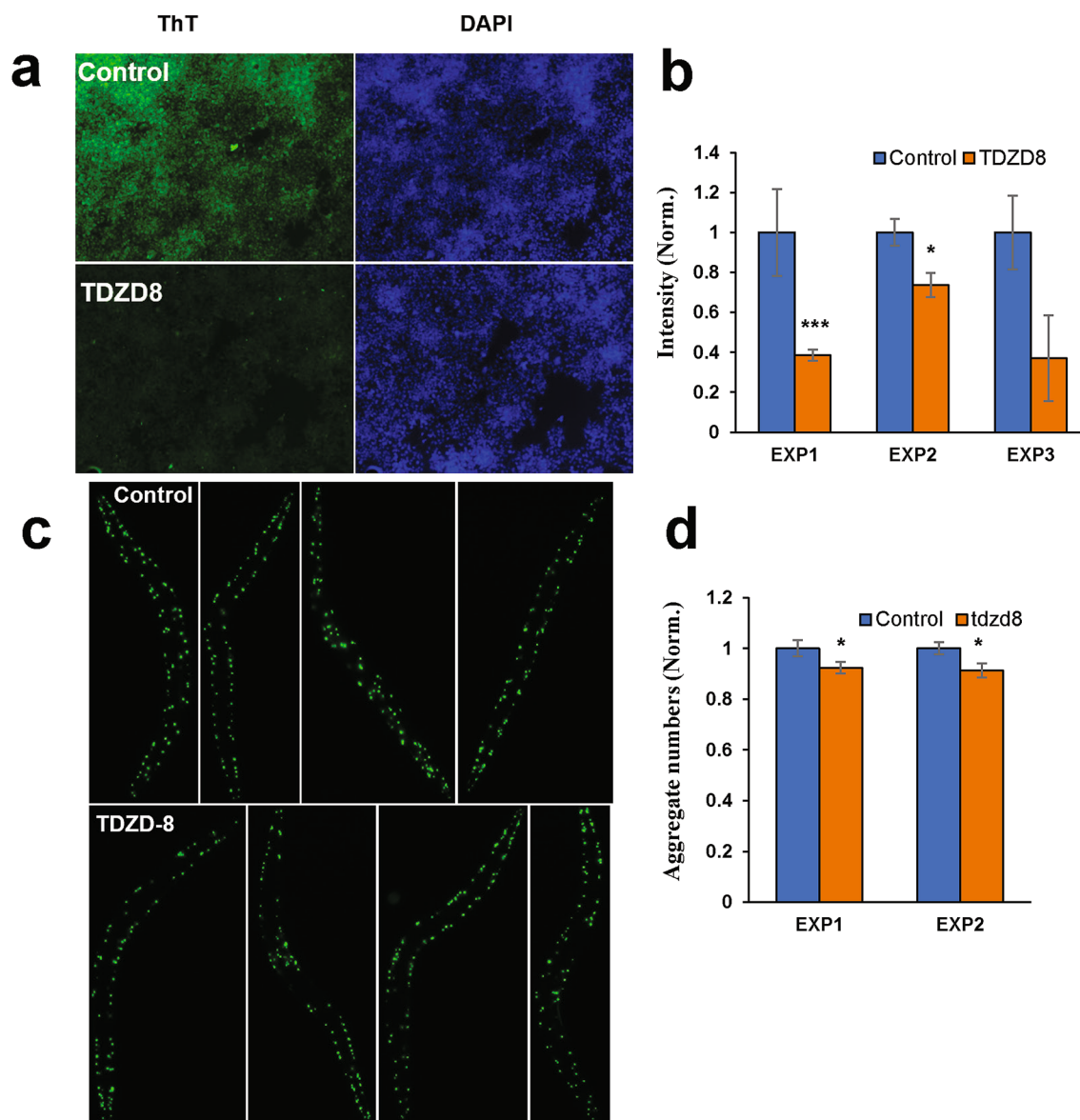


**Figure 3.** TDZD-8 treatment protects against amyloid-like aggregation in several model systems. **(a)** Thioflavin-T stains amyloid-like aggregates in HEK-tau cells, shown as controls (top panels) or after 48 h exposure to 5- $\mu$ M TDZD-8 (lower panels). **(b)** Normalized fluorescence intensities are shown for three independent experiments, in 2 of which treatment differed from control by 1-tailed *t*-test: \* $P < 0.05$ ; \*\*\* $P < 0.001$ . **(c)** Images of *C. elegans* adults (strain AM141, *unc-54p::Q40::yfp*) from the control group (top panel) or the drug-treated group (50- $\mu$ M TDZD-8) at day-5 post-hatch. **(d)** Normalized aggregate counts per worm,  $\pm$  SEM, were calculated and plotted for 10–12 worms per group in two independent experiments. Significance, calculated by 1-tailed *t*-tests: \* $P < 0.05$ .

Born model with solvent accessibility). For TDZD-8 docking to the inactive conformation of GSK3 $\beta$ ,  $\Delta G_{\text{binding}}$  was nearly twice that for the active conformation (Fig. 4e).

**Atomistic MD simulation shows stable TDZD-8 binding at the GSK3 $\beta$  hydrophobic pocket.** In order to evaluate the stability of TDZD-8 binding to the hydrophobic pocket of GSK3 $\beta$  in its inactive conformation, we conducted a 0.5- $\mu$ s, fully solvated atomistic molecular-dynamic simulation. The results indicate stable binding of TDZD-8 throughout the simulation. Snapshots taken at 100-ns intervals show continuous TDZD-8 occupation of the allosteric hydrophobic pocket between helix  $\alpha$ C of the *N*-terminal lobe and the catalytic domain (Fig. 4f). RMSD calculations indicate that GSK3 $\beta$  did not undergo major structural changes during the simulation (Fig. 4g; RMSD range is  $< 1$  Å for both the protein and ligand). RMSD trajectories for TDZD-8 complexed with GSK3 $\beta$  indicate stable drug binding in the hydrophobic pocket of GSK3 $\beta$  (Fig. 4g; dark red tracing). Since the number of amino acid-ligand contacts is crucial to the stability of a drug-protein complex, we monitored the interactions between TDZD-8 and GSK3 $\beta$  residues over time. TDZD-8 interacts throughout

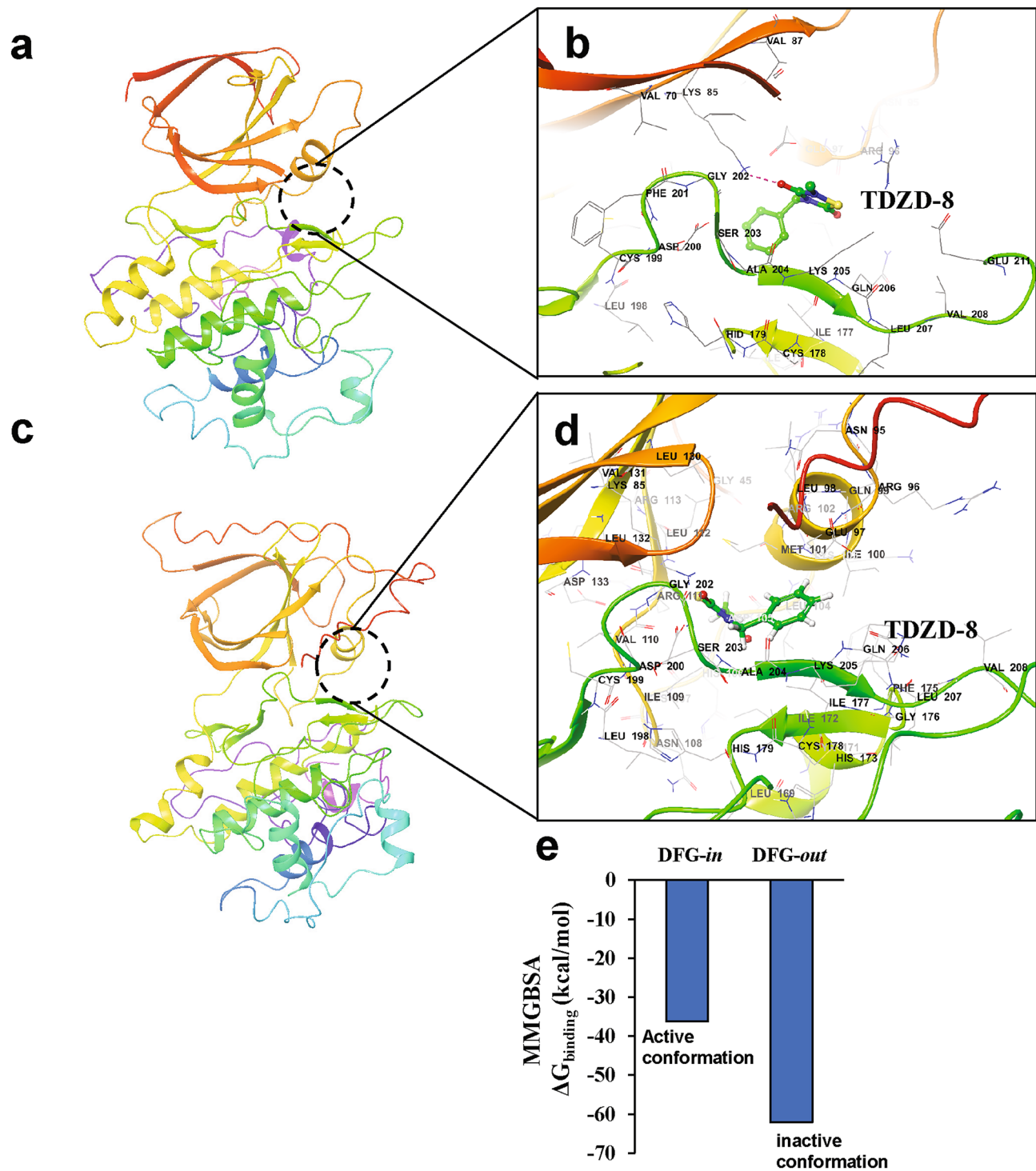


**Figure 4.** TDZD-8 binds to the allosteric hydrophobic pocket of GSK3 $\beta$ . (a,b) Glide docking pose of TDZD-8 binding to the GSK3 $\beta$  allosteric hydrophobic pocket in the modelled inactive DFG-out conformation. (c,d) TDZD-8 docked pose with modelled full-length GSK3 $\beta$ -pSer9 in the inactive DFG-out conformation. (e) MMGBSA-based  $\Delta G_{\text{binding}}$  (Gibbs free energy of binding) calculated for TDZD-8 with GSK3 $\beta$  in both active (DFG-in) and inactive (DFG-out) conformations. (f) Snapshots from 0.5- $\mu$ s simulation of full-length GSK3 $\beta$  (pSer9)-TDZD-8 complex taken at 100-ns intervals. (g) Root Mean Square Deviation of protein-ligand complex during a 0.5- $\mu$ s simulation; the blue and red tracings represent RMSD for GSK3 $\beta$  and TDZD-8, respectively. (h) Total number of contacts/interactions between TDZD-8 and GSK3 $\beta$  vs. time (top panel); stabilities of 16 individual interactions during the simulation (lower panel). Molecular structures are depicted with Schrödinger Maestro 11.4 (<https://www.schrodinger.com/>).

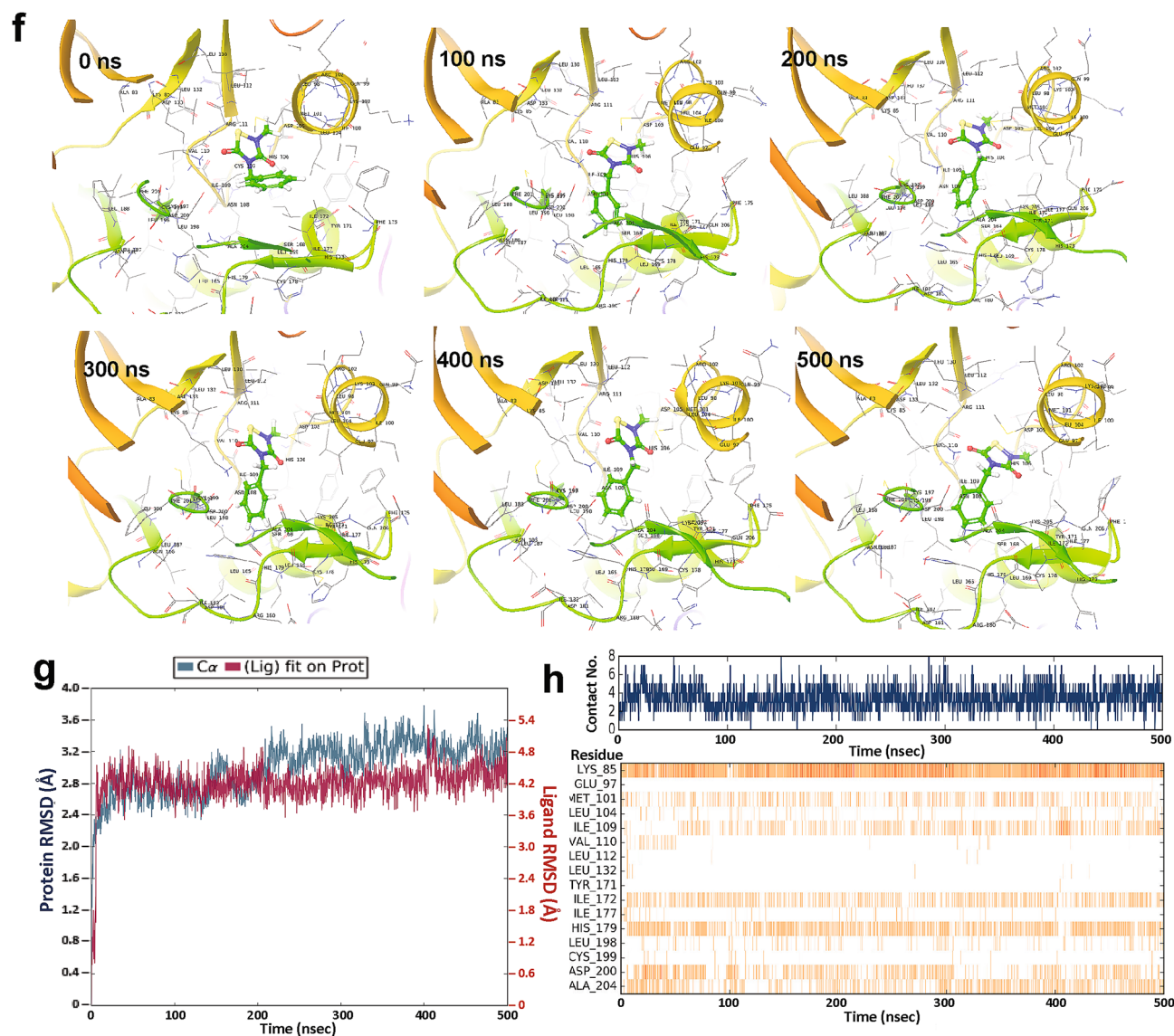


**Figure 4.** (continued)

most of the simulation with 2–6 GSK3 $\beta$  residues, averaging  $\sim 3$  (Fig. 4h). The most consistent contact residues were Lys85 and Asp200/Ala204.

**Computational docking and pharmacophore analysis of known inhibitors of GSK3 $\beta$  in the inactive conformation.** Since the discovery of TDZD-8, many inhibitors, including second-generation TDZD-8 analogs (e.g. TDZD-10 and Tideglusib), have been proposed and some of these were shown to be effective ATP-noncompetitive inhibitors of GSK3 $\beta$ <sup>20,30,31</sup>. However, the binding modes of these compounds were inadequately determined due to the lack of an empirically derived inactive conformation of GSK3 $\beta$ . In order to test the reliability of our predicted inactive conformation of GSK3 $\beta$ , we modeled the binding modes of previously known ATP-noncompetitive inhibitors of GSK3 $\beta$  against our predicted inactive conformation of GSK3 $\beta$ . These other known TDZD analogs that are ATP-noncompetitive inhibitors of GSK3 $\beta$  are predicted to bind at the hydrophobic pocket in the inactive conformation, with very high binding affinity (Fig. 5a). We tested Tideglusib, the best of the ATP-noncompetitive (TDZD) inhibitors of GSK3 $\beta$ , and showed that it binds at the interface between the *N*-terminal helix and the activation loop (i.e., in the hydrophobic/allosteric pocket), extending towards the active site (Fig. 5b). TDZD-10 (PubChemID:6539140; a.k.a. compound-45)<sup>31</sup> also fits well within the GSK3 $\beta$  hydrophobic pocket (Fig. 5c).

We next attempted to predict and model the common pharmacophore of TDZDs based on the protein–ligand complex we had modeled. Using Phase pharmacophore modeling from the Schrödinger suite, we predicted the pharmacophore of TDZD-8 when bound to GSK3 $\beta$  as a protein–ligand complex. The modeling algorithm proposed three key pharmacophore features (active components for target binding) for TDZD-8 binding (Fig. 5d): the TDZD ring (R3 in Fig. 5d) that participates in  $\pi$ -alkyl interactions, the carbonyl group attached to the TDZD ring (A2 in Fig. 5d) that forms an H-bond with Lys85, and the benzene ring (R4 in Fig. 5d) that participates in



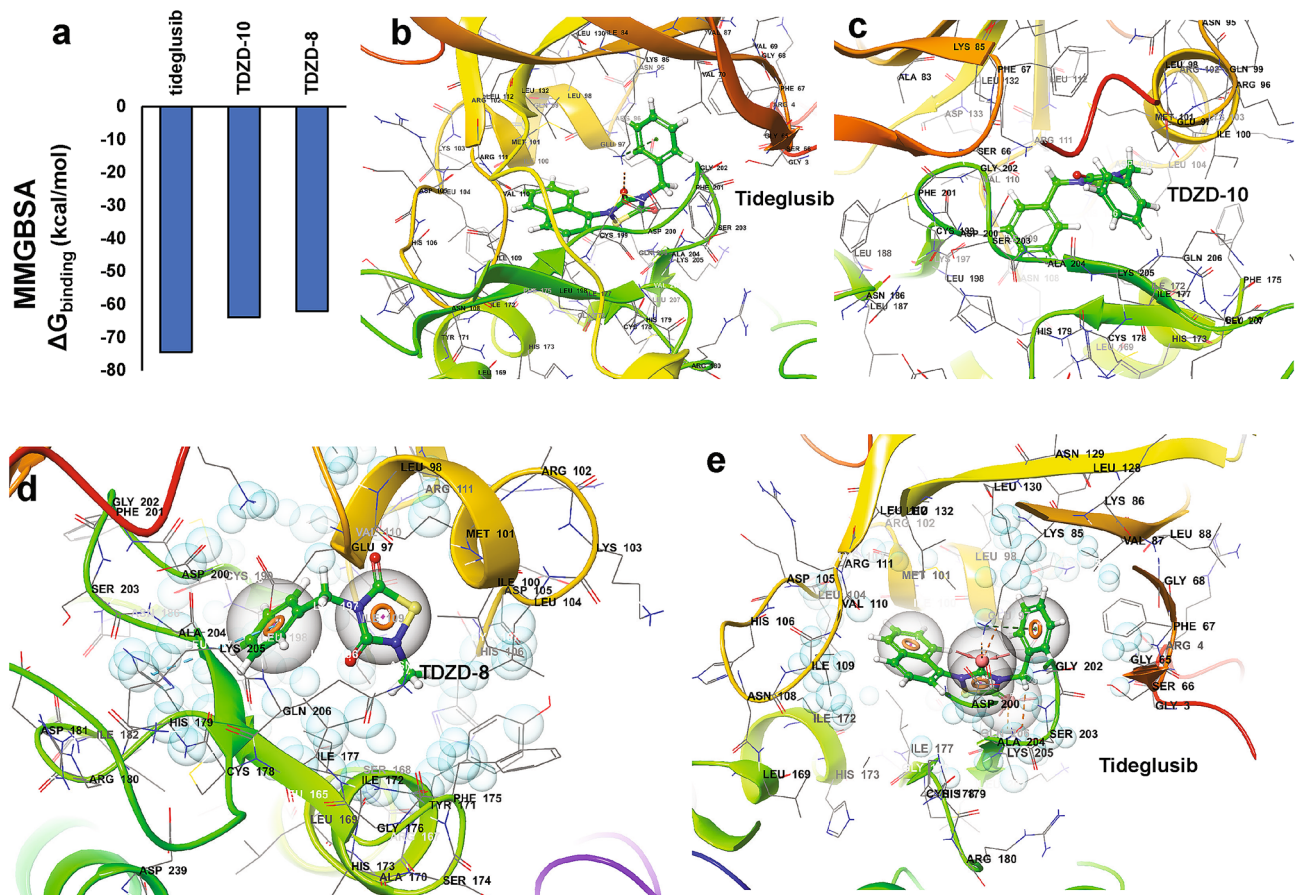


**Figure 5.** Binding modes of TDZD analogs with GSK3 $\beta$  inactive conformation. **(a)**  $\Delta G_{\text{binding}}$  (Gibbs free energy of binding), calculated by MMGBSA for 3 potent TDZD analogs, with GSK3 $\beta$  in the inactive conformation. **(b,c)** GSK3 $\beta$  docking poses with tideglusib and TDZD-10, indicate binding similar to that of TDZD-8 to the proposed allosteric hydrophobic pocket. **(d,e)** Pharmacophore modeling, based on predicted protein–ligand complexes, predicts key features involved in TDZD-8 and tideglusib binding. Molecular structures were created with Schrödinger Maestro 11.4 (<https://www.schrodinger.com/>).

$\pi$ -alkyl interactions. Pharmacophore modeling for Tideglusib, which targets the same reported critical residues in the activation loop (e.g. Lys205 and Asp200/Ala204), adds a naphthalene ring (R5) not present in TDZD-8, improving its binding affinity to GSK3 $\beta$  by adding  $\pi$ -alkyl bonds with Ile177 and Met101 (Fig. 5e). A comparison of the predicted pharmacophore features of the two TDZD analogs (TDZD-8, and Tideglusib) shows that the TDZD ring (R3) and carbonyl moiety (A2) remain the key common pharmacophore features of these TDZD analogs.

## Discussion

In this study, we modelled the inactive “DFG-out” conformation of GSK3 $\beta$  using metadynamic simulation (schematic representation; Supplementary Fig. 5). Previous studies showed that inhibition of GSK3 $\beta$  by a small-molecule drug blocks phosphorylation of tau and prevents its hyperphosphorylation—a step that initiates the formation of neurofibrillary tangles (NFT), the hallmark diagnostic feature of Alzheimer’s disease<sup>4,19,20,32</sup>. Many competitive inhibitors of GSK3 $\beta$  have been developed to target the catalytic (ATP-binding) site of the kinase in its active form/conformation, and are thus obliged to compete with ATP for binding<sup>33,34</sup>. Although GSK3 $\beta$  is often considered to be constitutively active, there is strong evidence that Ser9 phosphorylation induces kinase inactivation and inhibits substrate binding<sup>22,35,36</sup>, perhaps by favoring the DFG-out (inactive) conformation. Considering that GSK3 $\beta$  has the key DFG regulatory motif in its activation loop, in common with other Ser/Thr kinases, we hypothesized that Ser9 phosphorylation is likely to favor a flip to the inactive conformation, thereby inhibiting substrate binding.

Small molecules have been identified that inhibit the activity of a target kinase but do not compete with ATP for binding (i.e., they are non-competitive)<sup>19</sup>. In general, ATP-noncompetitive inhibitors are known to target an allosteric/hydrophobic pocket, observed in the inactive forms of several kinases<sup>9,37</sup>. Such inhibitors have two advantages over ATP-competitive inhibitors: (i) they often show greater target selectivity, since they do not bind to the active form of the kinase, evading the ATP-binding pocket that is largely conserved across the kinases; and (ii) they do not compete for binding with ATP at the ATP binding site on the active form of the kinase. ATP

is an abundant molecule with intracellular concentrations of 0.1–10 mM<sup>38</sup>, which has very high affinity for the ATP-binding sites of kinases in their active conformations.

TDZD-8 is an example of an ATP-noncompetitive inhibitor of GSK3 $\beta$ , and was proposed to target an allosteric hydrophobic pocket on the kinase<sup>19</sup>. TDZD analogs show relatively high specificity for GSK3 $\beta$ , resulting in potent inhibition and consequent amelioration of specific neuropathologies<sup>19,23</sup>. Several analogs of TDZD exhibit enhanced inhibitory activity against GSK3 $\beta$  relative to the parent compound<sup>20,31</sup>. Because GSK3 $\beta$  is widely considered to be constitutively active, it was long believed that TDZD analogs target an allosteric hydrophobic site in its active conformation. However, structural details of GSK3 $\beta$ 's interactions with TDZD-8 and its more potent analogs have eluded experimental resolution. Our computational analysis predicts that TDZD-8 would not show affinity for the active form of GSK3 $\beta$ , which appears to lack any allosteric hydrophobic pocket. This suggests that TDZD might instead bind to a hydrophobic pocket in the inactive form of the kinase, similar to Imatinib, another ATP-noncompetitive inhibitor that targets the inactive form of Abl kinase<sup>9</sup>. Prior to the current study, no experimentally determined structure had been reported for the inactive conformation of GSK3 $\beta$ , and very little was known about the binding modes or pharmacophores of TDZD-8 and its analogs. This gap in our knowledge has impeded the creation of next-generation TDZD analogs.

Atomistic metadynamic simulation has been a useful tool for predicting large conformational changes in the three-dimensional structures of proteins. We have applied metadynamic modeling to derive the inactive conformation of GSK3 $\beta$  from its known active conformation (based on X-ray crystallographic data<sup>10</sup>). Since metadynamics is an enhanced sampling method, it is able to predict conformational changes on a nanosecond scale, which is more than sufficient to predict the DFG-flip we observed at 18–25 ns. The predicted DFG-flip agrees with the available inactive conformations of other known kinases, including the Abl kinase structure empirically derived from X-ray data. Previous studies of other kinases have documented that the DFG-flip creates an allosteric pocket adjacent to the ATP binding site, consistent with cavities appearing in our predicted GSK3 $\beta$  inactive conformation, but absent from our starting model representing the active conformation. Another interesting feature of our predicted model is that the DFG-flip from an active to inactive state reduces the volume of the ATP-binding pocket. This corroborates previous evidence that ATP binding is attenuated upon kinase inactivation. At the same time, since non-competitive inhibitors are often stronger inhibitors of kinase activity<sup>9</sup>, novel non-competitive inhibitors can be identified by structure-based drug discovery using our predicted model.

Since phosphorylation of Ser9 plays a critical role in the activity of GSK3 $\beta$ , and the previously available experimental structures lack the *N*-terminal 35 residues, we first derived a full-length model of GSK3 $\beta$  structure in its active conformation. Metadynamic simulation showed that DFG-flip occurs spontaneously within the first few nanoseconds of simulation if Ser9 is phosphorylated. Interestingly, inactivation via DFG-flip was delayed when Ser9 was not phosphorylated, and the inactive conformation was unstable. This supports the hypothesis that Ser9 phosphorylation triggers inactivation of GSK3 $\beta$ . Apart from inhibiting substrate binding, Ser9 phosphorylation could also favor the DFG-flip to an inactive GSK3 $\beta$  conformation.

Computational docking of TDZD-8 with active-conformation GSK3 $\beta$  is not consistent with the previously proposed mode of TDZD-8 binding<sup>19</sup>. I.e., the proposed binding residues adjacent to the catalytic site cannot be reconciled with our docking model due to the absence of an allosteric hydrophobic pocket. Instead, the model predicts TDZD-8 binding to the proposed allosteric pocket of the inactive conformer of GSK3 $\beta$ . The predicted binding residues agree with previous reports for TDZD-8 binding, and thus support the predicted TDZD-8 binding to GSK3 $\beta$  in its inactive conformation. Additional support comes from the stronger affinity (more negative  $\Delta G_{\text{binding}}$ ) of TDZD-8 for GSK3 $\beta$  in the inactive rather than the active conformation. Molecular docking of other known GSK3 $\beta$  ATP-noncompetitive inhibitors predicts their modes of binding to the GSK3 $\beta$  inactive conformation. Interestingly, docking results predict that tideglusib, a potent and selective ATP-noncompetitive inhibitor of the thiazolidinone (TDZD) class of small molecules, should interact at the allosteric pocket of the GSK3 $\beta$  inactive conformation with high binding affinity relative to other known ATP-noncompetitive inhibitors, including palinurin and TDZD-10.

Interestingly, Tideglusib is known to inhibit GSK3 $\beta$  irreversibly<sup>20</sup>. This led to speculation that Tideglusib might form a covalent bond with Cys199 of GSK3 $\beta$ , but biochemical studies found no evidence of covalent linkage to Tideglusib at that residue<sup>20</sup>. Now, with the benefit of a structural model for the drug-protein complex, we have re-examined this putative mechanism of irreversible Tideglusib binding. Our structural model of GSK3 $\beta$  (inactive) binding by Tideglusib shows that the TDZD ring of Tideglusib does not face toward Cys199 (Fig. 5), making a covalent bond there unlikely. However, both modeling and docking studies of the Tideglusib-GSK3 $\beta$  (DFG-out) complex show the TDZD ring of Tideglusib in close proximity to Cys178 of GSK3 $\beta$ , in an orientation that could allow covalent-bond formation. Further biochemical studies will be required to test this possibility. Lead optimization of TDZD-8 analogs, based on a more compelling predicted binding mode, would provide significant assistance in designing more potent and selective inhibitors of GSK3 $\beta$  (manuscript in preparation). Results of the current study substantiate the important role of the GSK3 $\beta$  inactive conformation in the mechanism of non-competitive inhibition by TDZD-8 and its structural analogs.

## Methods

**Structure modeling and system building for MD runs.** The active (“DFG-in”) conformation of GSK3 $\beta$  was retrieved from the Protein Data Bank (PDB-ID **1I09**), from which we removed all crystal-associated water molecules and other heteroatoms associated with the structure. Prior to docking and simulation studies, GSK3 $\beta$  structure was preprocessed by adding missing hydrogens, side-chains, and loops, using the Protein Preparation Wizard within the Maestro Prime module (Schrodinger, Inc.). This preprocessed GSK3 $\beta$  active conformation was used for all further computational modeling studies in this manuscript. The active and inactive structure of c-Abl kinase were retrieved from Protein Data Bank (PDB-IDs **3KF4** and **3KFA** respectively).

Before simulations, the 3KF4 (active) structure of c-Abl kinase was loop refined and missing atoms/residues were added using Modeller V9.19.

**System building and metadynamic simulations.** The active conformation of GSK3 $\beta$ , prepared as above, was centered in an orthorhombic box positioned so that all box edges were 10-Å removed from the protein. This simulation box was solvated with Simple Point Charge (SPC) water and neutralized with Na<sup>+</sup>, Cl<sup>-</sup> counterions. NaCl at 0.15 M was then added to establish physiological salt concentration in the simulation box. The simulation system was then well equilibrated at 300°K using the NVT protocol with a Nose–Hoover chain thermostat. This was followed by another equilibration phase before the actual Molecular Dynamics (MD) run using the NPT protocol. The actual MD run followed a metadynamic simulation protocol as described previously<sup>11,39</sup>. Briefly, for the metadynamics run, collective variables (CVs) play crucial roles<sup>40</sup>. For our simulations, the distance between Phe 201 and Ser 168 in the GSK3 $\beta$  active structure (I109) was designated as a CV with Gaussian width of 0.05 Å. Simulations were conducted in GPU accelerated Desmond v2018.1 running on an NVIDIA Quadro P5000 cluster system developed in-house. Metadynamic simulations were conducted at a temperature of 300°K and pressure of 1.0 bar, with RESPA integrator.

**Atomistic molecular-dynamic simulations.** To analyze the stability of the protein–ligand complex, regular atomistic molecular-dynamic simulations were conducted using GPU accelerated Desmond v2018.1 with previously employed parameters<sup>26,41</sup>. Briefly, the protein–ligand complex was preprocessed as above using the Protein Preparation Wizard, and immersed in a orthorhombic box containing SPC water molecules. The simulation box was neutralized using Na<sup>+</sup>, Cl<sup>-</sup> as counterions with addition of 0.15-M NaCl as required. The well-equilibrated system was then simulated using the RESPA integrator at a temperature of 300°K and pressure of 1 bar. Trajectories were analyzed using the Simulation Interaction Diagram Generator from Desmond-Maestro.

**Molecular docking.** For unbiased docking, we used Linux-based Autodock-Vina with the Raccoon interface. The docking grid box was structured to cover the entire molecule, as described previously<sup>26,42</sup>. Target-specific (i.e. site-directed) docking and pose prediction were performed using the Glide docking interface within Maestro 2017-2 Suite (Schrodinger) running on a commercial license. The docking grid box was generated using the Receptor Grid Generator Wizard by manually selecting residues from either the active site or from the allosteric hydrophobic pocket. Docking calculations were performed in standard precision mode with flexible ligand sampling. Results were visualized and analyzed using the Maestro Viewer and Discovery Studio Visualizer.

**MMGBSA calculation of binding energy.** The docking pose from the Glide docking provided the initial input to calculate the solvent-based free energy of binding ( $\Delta G_{\text{binding}}$ ). Binding free energy of the input ligand was estimated by the MM-GBSA method (Molecular Mechanics using the Generalized Born model and Solvent Accessibility), as implemented in the Prime module of Schrodinger Suite.

**Pharmacophore modeling.** The output pose from Glide docking was used to generate a proposed pharmacophore based on the protein–ligand complex. The Auto E-pharmacophore method from the Phase plugin (Schrodinger Suite) was employed with default rules to formulate pharmacophore hypotheses, which were then visualized using Maestro Viewer.

**Strains, maintenance, and visualization of aggregates.** *C. elegans* strain AM141 [*unc-54p::Q40::yfp*] was obtained from the Caenorhabditis Genetics Center (CGC). This strain was maintained on a regular solid-agar nematode growth medium at 20 °C, seeded with OP50 (*E. coli*) bacteria. TDZD-8 compound was synthesized in-house and reconstituted as a stock solution in DMSO, which was then diluted in PBS and an amount was added to the agar plate 1–3 days prior to use, calculated to bring it to the working concentration specified in the paper once evenly diffused. Eggs from the well-fed AM141 strain were seeded onto control and experiment plates, maintained at 20 °C. Both controls and TDZD-8-treated worms, at day 5 post-hatch (approximately day 3 of adulthood), were imaged on a Keyence BZ-810 fluorescence microscope. Q40::YFP aggregates from the captured images were identified, counted, and quantified using Fiji image processing within ImageJ.

**Cell culture, maintenance, and thioflavin-T fluorescence assay.** Human embryonic kidney cells expressing human tau (HEK-tau) provided a model of human tauopathy, kindly provided by Dr. Brian Kraemer<sup>43</sup>. For regular maintenance, both cell types were plated at 250,000 cells per T-75 flask containing DMEM-F12 (1:1) supplemented with 10% v/v fetal bovine serum, and were maintained at 37 °C in a 5% CO<sub>2</sub> atmosphere with 95% relative humidity, in a tissue-culture incubator (FisherBrand). For experiments with drug treatment cells were plated at 6000 cells per well in a 96-well tissue culture treated plate (Costar). Drug-treated cells and controls were stained with thioflavin-T as previously described<sup>41,44,45</sup>. Cells were fixed after 48-h drug exposure, and incubated in phosphate-buffered saline containing 0.1% (w/v) thioflavin-T dye, and 4',6-diamidino-2-phenylindole (DAPI). After three successive 2-min washes, cells were imaged using a Keyence BZ-810 fluorescence microscope. After background subtraction at a rolling-ball radius of 50 (using Keyence image-analysis software), aggregate fluorescence was quantified from the images using Fiji (ImageJ).

**Statistical analyses.** The significance of differences between groups were calculated using the Behrens-Fisher heteroscedastic *t* test, appropriate to small samples ( $N=4$ ) for which the variance is poorly defined or

unequal. Single-tailed *t* tests are employed whenever the direction of change is known based on previous data; no Bonferroni correction has been applied, as only single endpoints were tested for intergroup significance.

## Data availability

The predicted inactive conformation of GSK3 $\beta$ , presented here, can be retrieved from this site: <https://data.mendeley.com/datasets/d69pzg3syh/1>.

Received: 10 July 2020; Accepted: 21 September 2020

Published online: 27 October 2020

## References

- Jellinger, K., Braak, H., Braak, E. & Fischer, P. Alzheimer lesions in the entorhinal region and isocortex in Parkinson's and Alzheimer's diseases. *Ann. N. Y. Acad. Sci.* **640**, 203–209. <https://doi.org/10.1111/j.1749-6632.1991.tb00218.x> (1991).
- Sirerol-Piquer, M. *et al.* GSK3 $\beta$  overexpression induces neuronal death and a depletion of the neurogenic niches in the dentate gyrus. *Hippocampus* **21**, 910–922. <https://doi.org/10.1002/hipo.20805> (2011).
- Mancinelli, R. *et al.* Multifaceted roles of GSK-3 in cancer and autophagy-related diseases. *Oxid. Med. Cell Longev.* **2017**, 4629495. <https://doi.org/10.1155/2017/4629495> (2017).
- Liu, F., Iqbal, K., Grundke-Iqbal, I. & Gong, C. X. Involvement of aberrant glycosylation in phosphorylation of tau by cdk5 and GSK-3 $\beta$ . *FEBS Lett.* **530**, 209–214. [https://doi.org/10.1016/s0014-5793\(02\)03487-7](https://doi.org/10.1016/s0014-5793(02)03487-7) (2002).
- Biernat, J. *et al.* The switch of tau protein to an Alzheimer-like state includes the phosphorylation of two serine-proline motifs upstream of the microtubule binding region. *EMBO J.* **11**, 1593–1597 (1992).
- Braak, H. & Braak, E. Neuropathological staging of Alzheimer-related changes. *Acta Neuropathol.* **82**, 239–259. <https://doi.org/10.1007/BF00308809> (1991).
- Griffin, W. S., Liu, L., Li, Y., Mrak, R. E. & Barger, S. W. Interleukin-1 mediates Alzheimer and Lewy body pathologies. *J. Neuroinflammation* **3**, 5. <https://doi.org/10.1186/1742-2094-3-5> (2006).
- Aboud, O. *et al.* Aging, Alzheimer's, and APOE genotype influence the expression and neuronal distribution patterns of microtubule motor protein dynactin-P50. *Front. Cell Neurosci.* **9**, 103. <https://doi.org/10.3389/fncel.2015.00103> (2015).
- Nagar, B. *et al.* Crystal structures of the kinase domain of c-Abl in complex with the small molecule inhibitors PD173955 and imatinib (STI-571). *Cancer Res.* **62**, 4236–4243 (2002).
- ter Haar, E. *et al.* Structure of GSK3 $\beta$  reveals a primed phosphorylation mechanism. *Nat. Struct. Biol.* **8**, 593–596. <https://doi.org/10.1038/89624> (2001).
- Lakkaniga, N. R., Balasubramaniam, M., Zhang, S., Frett, B. & Li, H. Y. Structural characterization of the aurora kinase B “DFG-flip” using metadynamics. *AAPS J.* **22**, 14. <https://doi.org/10.1208/s12248-019-0399-6> (2019).
- Vijayan, R. S. *et al.* Conformational analysis of the DFG-out kinase motif and biochemical profiling of structurally validated type II inhibitors. *J. Med. Chem.* **58**, 466–479. <https://doi.org/10.1021/jm501603h> (2015).
- Huse, M. & Kuriyan, J. The conformational plasticity of protein kinases. *Cell* **109**, 275–282. [https://doi.org/10.1016/s0092-8674\(02\)00741-9](https://doi.org/10.1016/s0092-8674(02)00741-9) (2002).
- Bellon, S. F. *et al.* c-Met inhibitors with novel binding mode show activity against several hereditary papillary renal cell carcinoma-related mutations. *J. Biol. Chem.* **283**, 2675–2683. <https://doi.org/10.1074/jbc.M705774200> (2008).
- MacAulay, K. *et al.* Constitutive activation of GSK3 down-regulates glycogen synthase abundance and glycogen deposition in rat skeletal muscle cells. *J. Biol. Chem.* **280**, 9509–9518. <https://doi.org/10.1074/jbc.M411648200> (2005).
- Cross, D. A., Alessi, D. R., Cohen, P., Andjelkovich, M. & Hemmings, B. A. Inhibition of glycogen synthase kinase-3 by insulin mediated by protein kinase B. *Nature* **378**, 785–789. <https://doi.org/10.1038/378785a0> (1995).
- Fang, X. *et al.* Phosphorylation and inactivation of glycogen synthase kinase 3 by protein kinase A. *Proc. Natl. Acad. Sci. USA* **97**, 11960–11965. <https://doi.org/10.1073/pnas.220413597> (2000).
- Tsujiro, I. *et al.* Inactivation of glycogen synthase kinase-3 by protein kinase C delta: implications for regulation of tau phosphorylation. *FEBS Lett.* **469**, 111–117. [https://doi.org/10.1016/s0014-5793\(00\)01234-5](https://doi.org/10.1016/s0014-5793(00)01234-5) (2000).
- Martinez, A., Alonso, M., Castro, A., Perez, C. & Moreno, F. J. First non-ATP competitive glycogen synthase kinase 3 beta (GSK-3 $\beta$ ) inhibitors: thiazolidinones (TDZD) as potential drugs for the treatment of Alzheimer's disease. *J. Med. Chem.* **45**, 1292–1299. <https://doi.org/10.1021/jm011020u> (2002).
- Dominguez, J. M. *et al.* Evidence for irreversible inhibition of glycogen synthase kinase-3 $\beta$  by tideglusib. *J. Biol. Chem.* **287**, 893–904. <https://doi.org/10.1074/jbc.M111.306472> (2012).
- Dodson, C. A. *et al.* Crystal structure of an Aurora-A mutant that mimics Aurora-B bound to MLN8054: insights into selectivity and drug design. *Biochem. J.* **427**, 19–28. <https://doi.org/10.1042/BJ20091530> (2010).
- Stamos, J. L., Chu, M. L., Enos, M. D., Shah, N. & Weis, W. I. Structural basis of GSK-3 inhibition by N-terminal phosphorylation and by the Wnt receptor LRP6. *Elife* **3**, e01998. <https://doi.org/10.7554/eLife.01998> (2014).
- Xie, C. L. *et al.* Inhibition of Glycogen Synthase Kinase-3 $\beta$  (GSK-3 $\beta$ ) as potent therapeutic strategy to ameliorates L-dopa-induced dyskinesia in 6-OHDA parkinsonian rats. *Sci. Rep.* **6**, 23527. <https://doi.org/10.1038/srep23527> (2016).
- Su, Y. *et al.* Lithium, a common drug for bipolar disorder treatment, regulates amyloid-beta precursor protein processing. *Biochemistry* **43**, 6899–6908. <https://doi.org/10.1021/bi035627j> (2004).
- Ryder, J. *et al.* Divergent roles of GSK3 and CDK5 in APP processing. *Biochem. Biophys. Res. Commun.* **312**, 922–929. <https://doi.org/10.1016/j.bbrc.2003.11.014> (2003).
- Janganati, V. *et al.* MMB triazole analogs are potent NF-kappaB inhibitors and anti-cancer agents against both hematological and solid tumor cells. *Eur. J. Med. Chem.* **157**, 562–581. <https://doi.org/10.1016/j.ejmech.2018.08.010> (2018).
- Guimaraes, C. R. & Cardozo, M. MM-GB/SA rescoring of docking poses in structure-based lead optimization. *J. Chem. Inf. Model* **48**, 958–970. <https://doi.org/10.1021/ci800004w> (2008).
- Balasubramaniam, M. *et al.* FCX-146, a potent allosteric inhibitor of Akt kinase in cancer cells: lead optimization of the second-generation arylidene indanone scaffold. *Biotechnol. Appl. Biochem.* <https://doi.org/10.1002/bab.1896> (2020).
- Castro, A. *et al.* Non-ATP competitive glycogen synthase kinase 3 $\beta$  (GSK-3 $\beta$ ) inhibitors: study of structural requirements for thiazolidinone derivatives. *Bioorg. Med. Chem.* **16**, 495–510. <https://doi.org/10.1016/j.bmc.2007.09.016> (2008).
- Nasim, S., Guzman, M. L., Jordan, C. T. & Crooks, P. A. Discovery of 1,2,4-thiazolidine-3,5-dione analogs that exhibit unusual and selective rapid cell death kinetics against acute myelogenous leukemia cells in culture. *Bioorg. Med. Chem. Lett.* **21**, 4879–4883. <https://doi.org/10.1016/j.bmcl.2011.06.027> (2011).
- Martinez, A. *et al.* SAR and 3D-QSAR studies on thiazolidinone derivatives: exploration of structural requirements for glycogen synthase kinase 3 inhibitors. *J. Med. Chem.* **48**, 7103–7112. <https://doi.org/10.1021/jm040895g> (2005).
- Lucas, J. J. *et al.* Decreased nuclear beta-catenin, tau hyperphosphorylation and neurodegeneration in GSK-3 $\beta$  conditional transgenic mice. *EMBO J.* **20**, 27–39. <https://doi.org/10.1093/emboj/20.1.27> (2001).

33. Leclerc, S. *et al.* Indirubins inhibit glycogen synthase kinase-3 beta and CDK5/p25, two protein kinases involved in abnormal tau phosphorylation in Alzheimer's disease. A property common to most cyclin-dependent kinase inhibitors?. *J. Biol. Chem.* **276**, 251–260. <https://doi.org/10.1074/jbc.M002466200> (2001).
34. Meijer, L. *et al.* Inhibition of cyclin-dependent kinases, GSK-3beta and CK1 by hymenialdisine, a marine sponge constituent. *Chem. Biol.* **7**, 51–63. [https://doi.org/10.1016/s1074-5521\(00\)00063-6](https://doi.org/10.1016/s1074-5521(00)00063-6) (2000).
35. Thornton, T. M. *et al.* Phosphorylation by p38 MAPK as an alternative pathway for GSK3beta inactivation. *Science* **320**, 667–670. <https://doi.org/10.1126/science.1156037> (2008).
36. Krishnankutty, A. *et al.* In vivo regulation of glycogen synthase kinase 3beta activity in neurons and brains. *Sci. Rep.* **7**, 8602. <https://doi.org/10.1038/s41598-017-09239-5> (2017).
37. Simard, J. R. *et al.* High-throughput screening to identify inhibitors which stabilize inactive kinase conformations in p38alpha. *J. Am. Chem. Soc.* **131**, 18478–18488. <https://doi.org/10.1021/ja907795q> (2009).
38. Schrier, S. M. *et al.* Extracellular adenosine-induced apoptosis in mouse neuroblastoma cells: studies on involvement of adenosine receptors and adenosine uptake. *Biochem. Pharmacol.* **61**, 417–425. [https://doi.org/10.1016/s0006-2952\(00\)00573-6](https://doi.org/10.1016/s0006-2952(00)00573-6) (2001).
39. Balasubramaniam, M. *et al.* Interleukin-1beta drives NEDD8 nuclear-to-cytoplasmic translocation, fostering parkin activation via NEDD8 binding to the P-ubiquitin activating site. *J. Neuroinflammation* **16**, 275. <https://doi.org/10.1186/s12974-019-1669-z> (2019).
40. Park, J., McDonald, J. J., Petter, R. C. & Houk, K. N. Molecular Dynamics Analysis of Binding of Kinase Inhibitors to WT EGFR and the T790M Mutant. *J. Chem. Theory Comput.* **12**, 2066–2078. <https://doi.org/10.1021/acs.jctc.5b01221> (2016).
41. Balasubramaniam, M., Ayyadevara, S. & Shmookler Reis, R. J. Structural insights into pro-aggregation effects of *C. elegans* CRAM-1 and its human ortholog SERF2. *Sci. Rep.* **8**, 14891. <https://doi.org/10.1038/s41598-018-33143-1> (2018).
42. Bommagani, S. *et al.* A novel tetrazole analogue of resveratrol is a potent anticancer agent. *Bioorg. Med. Chem. Lett.* **29**, 172–178. <https://doi.org/10.1016/j.bmcl.2018.12.006> (2019).
43. Wheeler, J. M., Guthrie, C. R. & Kraemer, B. C. Potential neuroprotective strategies against tauopathy. *Biochem. Soc. Trans.* **40**, 656–660. <https://doi.org/10.1042/BST20120017> (2012).
44. Ayyadevara, S. *et al.* Aspirin-mediated acetylation protects against multiple neurodegenerative pathologies by impeding protein aggregation. *Antioxid Redox Signal* **27**, 1383–1396. <https://doi.org/10.1089/ars.2016.6978> (2017).
45. Balasubramaniam, M. *et al.* Aggregate interactome based on protein cross-linking interfaces predicts drug targets to limit aggregation in neurodegenerative diseases. *iScience* **20**, 248–264. <https://doi.org/10.1016/j.isci.2019.09.026> (2019).

## Acknowledgements

This work was supported by grants from the National Institute on Aging (NIA/NIH grants R01 AG062254-01 [R] Shmookler Reis & S Ayyadevara, co-PIs) and P01 AG012411-17A1 [WST Griffin, PI]), and from the U.S. Dept. of Veteran Affairs (BLR&D Merit Grant BX001655 [R] Shmookler Reis, PI) and BLR&D SRCSA Grant IK6 BX004851 [R] Shmookler Reis, PI]), and from the Inglewood Scholars Program [M.B. awardee].

## Author contributions

M.B. and R.J.S.R. planned the study. M.B. performed computational modeling and simulations with contributions from N.M., who also performed cell culture experiments. P.A. performed *C. elegans* experiments with guidance from S.A. S.K.B. synthesized small molecules with guidance from N.R.P. and P.A.C. M.B. and R.J.S.R. wrote the manuscript, with additional input from P.A.C.

## Competing interests

The authors declare no competing interests.

## Additional information

**Supplementary information** is available for this paper at <https://doi.org/10.1038/s41598-020-75020-w>.

**Correspondence** and requests for materials should be addressed to M.B. or R.J.S.R.

**Reprints and permissions information** is available at [www.nature.com/reprints](http://www.nature.com/reprints).

**Publisher's note** Springer Nature remains neutral with regard to jurisdictional claims in published maps and institutional affiliations.



**Open Access** This article is licensed under a Creative Commons Attribution 4.0 International License, which permits use, sharing, adaptation, distribution and reproduction in any medium or format, as long as you give appropriate credit to the original author(s) and the source, provide a link to the Creative Commons licence, and indicate if changes were made. The images or other third party material in this article are included in the article's Creative Commons licence, unless indicated otherwise in a credit line to the material. If material is not included in the article's Creative Commons licence and your intended use is not permitted by statutory regulation or exceeds the permitted use, you will need to obtain permission directly from the copyright holder. To view a copy of this licence, visit <http://creativecommons.org/licenses/by/4.0/>.

This is a U.S. Government work and not under copyright protection in the US; foreign copyright protection may apply 2020